

## Heavy-Ion Physics

A. Ayala

Instituto de Ciencias Nucleares, Universidad Nacional Autónoma de México, CdMx 04510, México, and Centre for Theoretical and Mathematical Physics, University of Cape Town, South Africa.

### Abstract

The field of relativistic heavy-ion physics has become an important testing ground for our current understanding of the properties of strongly interacting matter under extreme conditions. Strong interactions are described by Quantum Chromodynamics which, in addition to its defining gauge symmetry, possesses additional symmetries and properties that can be put to test in collisions of heavy-nuclei at different beam energies. The exploration of these properties is currently being conducted and will still continue for years to come when new facilities enter into operation. This is the so called study of the QCD phase diagram. Of particular relevance is the search of a possible critical end point (CEP). In these lectures I make a brief survey of QCD properties and of its symmetries. Since the phase diagram refers to the study of phase transitions, I also give the main generalities of such and mention some of the statistical tools than can be used to study the fluctuations in conserved charges to identify the CEP location. I also give a brief summary of some of the experimental signals used to study the properties of the kind of matter created in heavy-ion collisions at the highest available energy, the so called Quark Gluon Plasma.

### 1 Introduction

The field of relativistic heavy-ion physics has become the main playground to explore the properties of hadron matter under extreme conditions of temperature and density. Experimentally, the relativistic heavy-ion program started out at modest energies in the mid-1980s, when collisions of heavy-nuclei, in fixed target experiments with center-of-mass energy of 5 and 17 GeV per nucleon pair, were carried out at the Alternating Gradient Synchrotron (AGS) in Brookhaven and the Super Proton Synchrotron (SPS) at CERN, respectively. Shortly before the turn of the century, the relativistic heavy-ion program got a new boost when the Relativistic Heavy-Ion Collider (RHIC) in Brookhaven started to collide gold nuclei at a, by then unprecedented, center-of-mass energy of 200 GeV per nucleon pair. At the end of 2010, the first collisions of lead nuclei were delivered by the Large Hadron Collider at CERN, at a center-of-mass energy of 2.76 TeV per nucleon pair. By the end of 2015, the LHC was able to increase this energy to 5.02 TeV. The exciting results obtained from experiments measuring the properties of the hot and dense matter created in these collisions offer a better shaped but still incomplete picture of the properties of strongly interacting matter under extreme conditions. The program promises to keep producing new and equally exciting results when facilities such as NICA, FAIR, J-PARC and KEK, designed to explore the properties of this kind of matter at higher baryon densities, enter into operation.

The purpose of these lecture notes is to provide a theoretical framework, at the introductory level, to put into context the aim and meaning of some of the results of the experimental program. I focus on the description of the different phases that strongly interacting matter can reach when its temperature and baryon density are varied by varying the center-of-mass energy in the collisions. These phases can be better described in terms of an idealized picture based on the so called *QCD Phase Diagram*, where

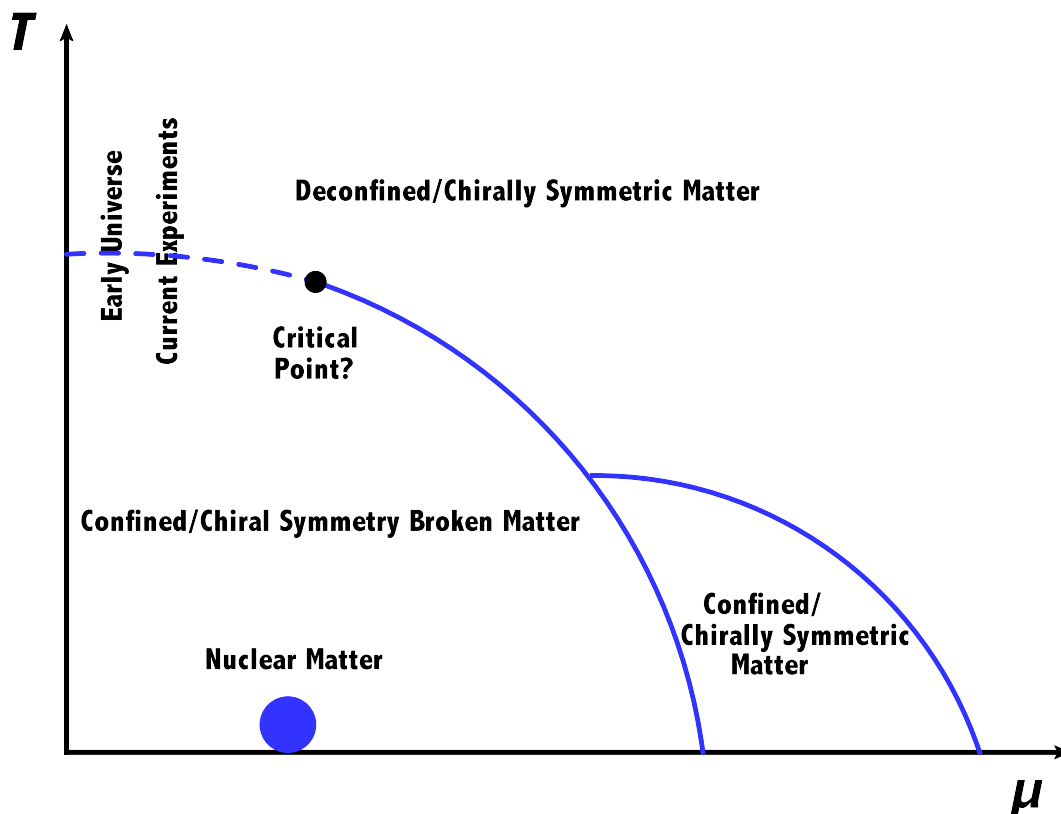


**Figure 1:** Representation of the QCD phase diagram in the temperature ( $T$ ) and quark chemical potential ( $\mu$ ) plane.

the transition lines correspond to the boundaries between one and another phase. Figure 1 shows a representation of this phase diagram. Close to the phase boundaries, the relevant quark species are the light quarks  $u$ ,  $d$  and  $s$ . A complete description, accounting for the abundance of these species, should in principle be given in terms of the chemical potentials associated to each of these quarks. Nevertheless, when one assumes equilibrium, these chemical potentials are not independent from each other. They are related by the requirements of beta equilibrium and charge neutrality. Therefore, out of the three chemical potentials only one is independent. Any one of them can be chosen and the usual choice is the baryon chemical potential  $\mu_B$ , related to the quark chemical potential  $\mu$  by  $\mu = \mu_B/3$ .

The transit through the phase boundaries is related to the restoration/breaking of QCD symmetries and thus an account of such symmetries is the main unifying concept along the text. The lectures are organized as follows: In Sec. 2, I focus on the description of QCD flavor and chiral symmetries. In Sec. 3 I discuss the main features of QCD confinement and asymptotic freedom. In Sec. 4 I describe how chiral symmetry/deconfinement are restored in heavy-ion collisions at high energy. Since the description is made in terms of thermodynamical quantities, I recall the concept of phase transitions and provide a survey of our current knowledge of the QCD phase structure obtained from lattice QCD (LQCD). I also discuss how the search for the QCD critical end point is a central subject in the field and some of the theoretical tools to try to identify this point from experimental measurements. In Sec. 5 I discuss some

of the experimental signals that give an account of our current understanding of the properties of the deconfined state of matter produced in heavy-ion reactions, generally known as the quark-gluon plasma (QGP). I finally summarize in Sec. 6.

## 2 Flavor and chiral symmetries [1]

The quantum field theory that describes strong interactions is Quantum Chromodynamics (QCD). This is a gauge theory based on the local symmetry group  $SU(N_c)$ , where  $N_c$  is the number of colors. In Nature  $N_c = 3$ . The fundamental fields are the quarks (matter fields) and the gluons (gauge fields). Each one of the  $N_f$  quark fields belong to the fundamental representation of the color group which is  $N_c$ -dimensional. The antiquark fields belong to the complex conjugate of the fundamental representation, also  $N_c$ -dimensional and the gluon fields to the adjoint representation, which is  $N_c^2 - 1$ -dimensional.

The QCD Lagrangian at the classical level is written as

$$\mathcal{L}_{QCD} = \sum_{i=1}^{N_f} \bar{\psi}_i^a \left( i\gamma^\mu (\partial_\mu \delta^{ab} + ig_s A_\mu^{ab}) - m_i \delta^{ab} \right) \psi_i^b - \frac{1}{4} G_{\mu\nu}^\alpha G_\alpha^{\mu\nu} \quad (1)$$

where  $G_{\mu\nu}^\alpha = \partial_\mu A_\nu^\alpha - \partial_\nu A_\mu^\alpha + g_s f^{\alpha\beta\sigma} A_\mu^\beta A_\nu^\sigma$ ,  $A_\mu^{ab} = A_\mu^\sigma (\tau_\sigma)^{ab}$  with  $a, b = 1, \dots, N_c$  and  $\alpha, \beta, \sigma = 1, \dots, N_c^2 - 1$ .  $g_s$  is the coupling strength both between matter and gauge fields and between gauge fields themselves,  $m_i$  is the (bare) mass for each quark flavor and  $\tau_\sigma$  are the generators of the  $SU(N_c)$  algebra. For  $N_c = 3$ , these are usually taken as the Gell-Mann matrices.

Quarks are distinguished from one another by a quantum number called *flavor*. There are six flavors:  $u, d, s, c, b, t$ . and we refer to the number of flavors generically as  $N_f$ . Consider the ideal case in which all  $N_f$  flavors have the same mass. Quark and antiquark fields are assigned to the fundamental and complex conjugate representations (each  $N_f$ -dimensional), respectively, of the  $SU(N_f)$  group. The Lagrangian corresponding to the quark sector becomes (we omit color indices for quarks and gluons)

$$\mathcal{L}_q = \sum_{i=1}^N \bar{\psi}_i (i\gamma^\mu (\partial_\mu + ig_s A_\mu) - m) \psi_i \quad (2)$$

$\mathcal{L}_q$  is invariant under continuous *global transformations* of  $SU(N_f)$

$$\begin{aligned} \psi_i &\longrightarrow \psi'_i = e^{-i\alpha^A (T^A)_i^j} \psi_j \\ \bar{\psi}_i &\longrightarrow \bar{\psi}'_i = \bar{\psi}_j e^{i\alpha^A (T^A)_i^j} \\ A_\mu &\longrightarrow A'_\mu = A_\mu, \end{aligned} \quad (3)$$

$A = 1, \dots, N_f^2 - 1$ ,  $T^A$  are  $N_f \times N_f$  matrices.

In infinitesimal form

$$\begin{aligned} \delta \psi_i &= -i\delta\alpha^A (T^A)_i^j \psi_j \\ \delta \bar{\psi}_i &= i\delta\alpha^A \bar{\psi}_j (T^A)_i^j \\ \delta A_\mu &= 0. \end{aligned} \quad (4)$$

Using Noether's theorem, one finds  $N_f^2 - 1$  conserved currents

$$\begin{aligned} j_\mu^A(x) &= \bar{\psi}_i(x) \gamma_\mu (T^A)_i^j \psi^i(x) \\ \partial^\mu j_\mu^A &= 0. \end{aligned} \quad (5)$$

The generators of the group (the charges) are obtained from  $j_0^A$  by space integration

$$Q^A = \int d^3x j_0^A(x). \quad (6)$$

$Q^A$ 's satisfy the  $SU(N_f)$  algebra

$$[Q^A, Q^B] = if^{ABC} Q^C, \quad (7)$$

$A, B, C = 1, \dots, N_f^2 - 1$ . Current conservation implies that the generators are independent of time and therefore they commute with the Hamiltonian  $H$

$$[H, Q^A] = 0. \quad (8)$$

The transformation properties of the fields can be translated to the states. Introduce one-particle quark states (omit spin labels)  $|\mathbf{p}, i\rangle$ . If the vacuum state is invariant under the group transformations, then

$$Q^A |\mathbf{p}, i\rangle = (T^A)_i^j |\mathbf{p}, j\rangle. \quad (9)$$

Since these states are also eigenstates of the Hamiltonian, the above means that the various one-particle states of the fundamental representation multiplet have equal masses  $m$ . This mode to realize the symmetry is called the *Wigner-Weyl* mode.

Consider however the real case where flavors have different masses

$$\mathcal{L}_q = \sum_{i=1}^N \bar{\psi}_i (i\gamma^\mu (\partial_\mu + ig_s A_\mu) - m_i) \psi_i. \quad (10)$$

The mass term spoils  $SU(N_f)$  invariance, therefore currents are not conserved and we find

$$\partial^\mu j_\mu^A = -i \sum_{i,j=1}^{N_f} (m_i - m_j) \bar{\psi}_i (T^A)_i^j \psi_j \neq 0 \quad (11)$$

In Nature, quarks are divided into two groups: *Light quarks*  $u, d, s$  and *heavy quarks*  $c, b, t$ . The mass difference between each group is large ( $> 1$  GeV). An approximate symmetry can be expected only for the light quarks:  $SU(2)$  for  $u, d$  or  $SU(3)$  for  $u, d, s$ .

Notice that quarks can also be transformed by means of unitary transformations that include the  $\gamma_5$  matrix. The transformations are called *axial flavor transformations*. In infinitesimal form

$$\begin{aligned} \delta \psi_i &= -i\delta\alpha^A (T^A)_i^j \gamma_5 \psi_j \\ \delta \bar{\psi}_i &= i\delta\alpha^A \bar{\psi}_j \gamma_5 (T^A)_i^j \\ \delta A_\mu &= 0. \end{aligned} \quad (12)$$

Consider the quark part of the Lagrangian  $\mathcal{L}_q$  with equal masses. Under these transformations  $\mathcal{L}_q$  is not invariant because of the mass

$$\delta \mathcal{L}_q = 2im\delta\alpha^A \bar{\psi}^i (T^A)_i^j \gamma_5 \psi_j. \quad (13)$$

Invariance under axial flavor transformations requires vanishing of the quark mass. Contrary to flavor symmetry transformations, equality of masses is not sufficient for invariance under axial flavor transformations. In the general case of different masses, we introduce the *mass matrix*  $\mathcal{M} = \text{diag}(m_1, m_2, \dots, m_{N_f})$ . The variation of the Lagrangian is

$$\delta \mathcal{L}_q = i\delta\alpha^A \bar{\psi}^i \{M, T^A\}_i^j \gamma_5 \psi_j, \quad (14)$$

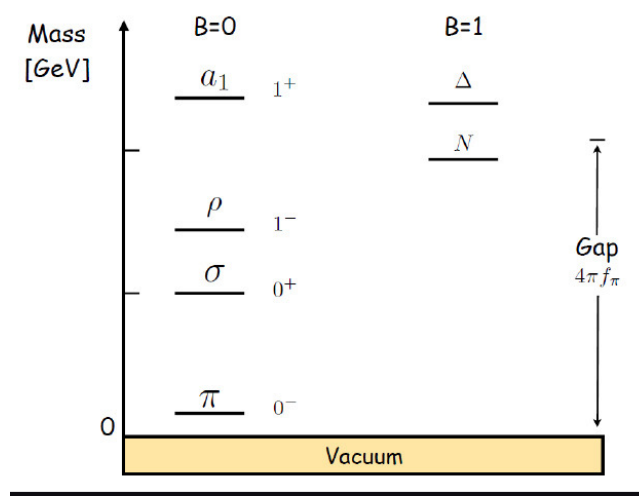


**Figure 2:** Schematic representation of the parity doublets for the lightest meson and baryon states.

where  $\{, \}$  is the anticommutator.

Consider the massless case. The Lagrangian is invariant under both the flavor and the axial flavor transformations. The conserved currents are

$$\begin{aligned} j_\mu^A(x) &= \bar{\psi}_i(x) \gamma_\mu (T^A)^i_j \psi^j(x); & \partial^\mu j_\mu^A &= 0 \\ j_{5\mu}^A(x) &= \bar{\psi}_i(x) \gamma_\mu \gamma_5 (T^A)^i_j \psi^j(x); & \partial^\mu j_{5\mu}^A &= 0. \end{aligned} \quad (15)$$

The corresponding charges are

$$Q^A = \int d^3x j_0^A(x), \quad Q_5^A = \int d^3x j_{50}^A(x). \quad (16)$$

Together the flavor and axial flavor transformations form the *chiral transformations*. The corresponding charges satisfy the commutation relations

$$[Q^A, Q^B] = if^{ABC} Q^C, \quad [Q^A, Q_5^B] = if^{ABC} Q_5^C, \quad [Q_5^A, Q_5^B] = if^{ABC} Q^C. \quad (17)$$

The axial charges do not form an algebra, however, if we define

$$Q_L^A = \frac{1}{2}(Q^A - Q_5^A), \quad Q_R^A = \frac{1}{2}(Q^A + Q_5^A) \quad (18)$$

we obtain

$$[Q_L^A, Q_L^B] = if^{ABC} Q_L^C, \quad [Q_R^A, Q_R^B] = if^{ABC} Q_R^C, \quad [Q_L^A, Q_R^B] = 0. \quad (19)$$

The result can be summarized as follows: The left-handed and right-handed charges decouple and operate separately. Each generate an  $SU(N_f)$  group. The chiral group is decomposed into the direct product of two  $SU(N_f)$  groups, labeled with the subscripts  $L$  and  $R$ , *i.e.* the chiral group =  $SU(N_f)_L \otimes SU(N_f)_R$ . In Nature, chiral symmetry is not exact, *quark masses break it explicitly*. In the light quark sector, the breaking can be treated as a perturbation, the symmetry is approximate. What is the signature of this approximate symmetry?

Suppose that the symmetry is realized in the Wigner-Weyl mode. Thus, in the massless quark limit a chiral transformation acting on a massive state gives

$$Q_5^A |M, s, \mathbf{p}, +, i\rangle = (T^A)^j_i |M, s, \mathbf{p}, -, j\rangle. \quad (20)$$

This means that we should find parity partners for the massive states. When we consider the light quark masses, the degeneracy within parity doublets is lifted, but the masses should remain close to each other. No degenerate parity doublets are observed, thus the Wigner-Weyl mode realization of chiral symmetry does not happen under ordinary conditions. The alternative is spontaneous symmetry breaking, also known as Nambu-Goldstone mode. What happens if the generators of some transformations do not annihilate the vacuum?

$$Q_5^A |0\rangle \neq 0. \quad (21)$$

In this case we say that the symmetry has been spontaneously broken. The axial charges when applied to the vacuum state produce new states

$$Q_5^A |0\rangle = |A, -\rangle, \quad A = 1, \dots, N_f^2 - 1 \quad (22)$$

The states have the same properties as the axial charges that generate it, in particular they are *pseudoscalar* states.

In the massless limit, the charges commute with the Hamiltonian therefore, these states are massless (Goldstone theorem). Spontaneous chiral symmetry breaking is manifested by means of the existence of  $N_f^2 - 1$  pseudoscalar massless particles called Nambu-Goldstone bosons. The breaking of the symmetry involves only the axial sector. The ordinary flavor symmetry is still realized in the Wigner-Weyl mode.

$$SU(N_f)_L \otimes SU(N_f)_R \longrightarrow SU(N_f)_V. \quad (23)$$

In Nature  $N_f = 3$ , this corresponds to eight pseudoscalar bosons ( $\pi, K, \eta$ ) with small masses.

We have thus seen that chiral symmetry is broken due to a finite mass of the quarks. Under ordinary circumstances, quarks are confined within hadrons. The quark mass is thus an *effective* mass which corresponds to about one third of the nucleon mass  $\sim 300$  MeV. The origin of this effective, or dynamically generated mass, is the strength of the interaction and can be explained in terms of non-perturbative methods [2]. It seems intuitively clear that if we could somehow overcome the confining of quarks, their mass would decrease and chiral symmetry would be *restored*. Let us now study how the strong interaction produces this confinement to later ask how a collision of relativistic nuclei could help to study the situation where quiral symmetry and deconfinement are achieved.

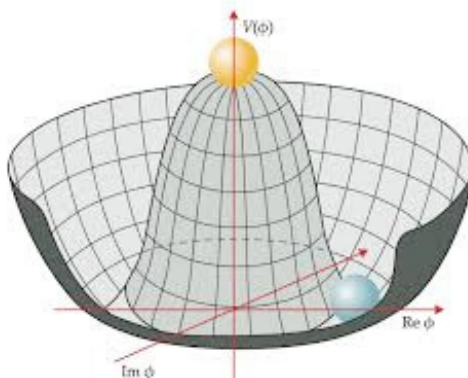


**Figure 3:** Schematic representation of spontaneous symmetry breaking. Goldstone bosons correspond to the directions where the potential is flat.

### 3 Confinement and asymptotic freedom

To grasp why under ordinary circumstances quarks are confined within hadrons let us recall the characteristics of the strong interaction: The potential between two quarks at “long” distances,  $\mathcal{O}(1 \text{ fm})$ , is linear, this means that the separation of quarks requires “infinite” amount of energy. Confinement is a direct consequence of the gluon self-interaction. Quarks and gluons confined inside the QCD potential must combine into zero net color charge particles called hadrons.

The strength of strong interaction is characterized by a coupling “constant”  $\alpha_s = g_s^2/4\pi$  whose strength decreases with distance since the bare color charge is *antiscreened* due to gluon self-interaction. To study confinement and the *running* of the strong coupling with distance (or equivalently, with the energy involved in the physical process), one resorts to a renormalization group analysis of the gluon polarization tensor

$$\Pi^{\mu\nu}(q) = \Pi(q^2, \alpha_s) \left( g^{\mu\nu} - \frac{q^\mu q^\nu}{q^2} \right), \quad (24)$$

where we refer to  $\Pi$  as the gluon self-energy. Gauge invariance dictates that the gluon polarization tensor be transverse and thus the tensor structure in Eq. (24). Let  $\Pi(q^2)$  represent the un-renormalized gluon self-energy. Let us scale each factor of the momentum  $q$  appearing in  $\Pi$  by the renormalization ultraviolet energy scale  $\tilde{\mu}$ , writing

$$q^2 = \tilde{\mu}^2 (q^2/\tilde{\mu}^2). \quad (25)$$

Therefore, we have

$$\Pi(q^2; \alpha_s) = \tilde{\mu}^D \Pi(q^2/\tilde{\mu}^2; \alpha_s), \quad (26)$$

where  $D = 2$  is the energy dimension of  $\Pi$ . Since  $\tilde{\mu}$  is arbitrary, the statement that  $\Pi$  should be independent of this scale is provided by the Renormalization Group Equation (RGE) [3]

$$\left( \tilde{\mu} \frac{\partial}{\partial \tilde{\mu}} + \alpha_s \beta(\alpha_s) \frac{\partial}{\partial \alpha_s} - \gamma \right) \Pi(q^2; \alpha_s) = 0, \quad (27)$$

where  $\beta(\alpha_s)$  is the QCD beta function defined by

$$\alpha_s \beta(\alpha_s) = \tilde{\mu} \frac{\partial \alpha_s}{\partial \tilde{\mu}}, \quad (28)$$

and

$$\gamma = \tilde{\mu} \frac{\partial}{\partial \tilde{\mu}} \ln Z^{-1}, \quad (29)$$

where  $Z$  is the gluon self-energy renormalization. The beta function represents the rate of change of the renormalized coupling as the renormalization scale  $\tilde{\mu}$  is increased. The dependence of a given Green’s function on  $\tilde{\mu}$  happens through the counter-terms that subtract ultraviolet divergences. Therefore, the beta function can be computed from the counter-terms that enter a properly chosen Green’s function. In QCD, to lowest order, the beta function can be computed as

$$\beta = g_s \tilde{\mu} \frac{\partial}{\partial \tilde{\mu}} \left( -\delta_1 + \delta_2 + \frac{1}{2} \delta_3 \right) \quad (30)$$

where  $\delta_1$ ,  $\delta_2$  and  $\delta_3$  are the counter-terms for the quark-gluon vertex, the quark self-energy and the gluon self-energy [4]. The QCD beta function is negative and to one-loop level it is given by

$$\beta(\alpha_s) = -b_1 \alpha_s, \quad b_1 = \frac{1}{12\pi} (11N_c - 2N_f) > 0. \quad (31)$$

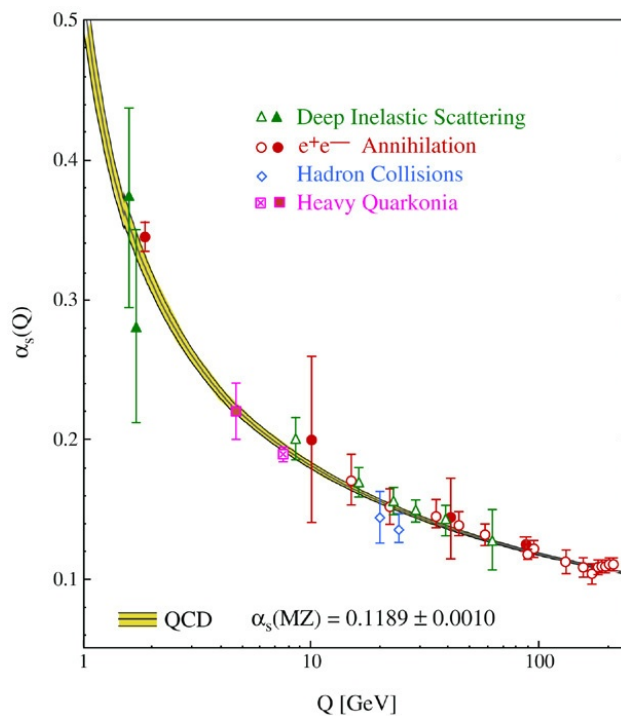


**Figure 4:** Running of  $\alpha_s$  as a function of the momentum transferred  $Q$  in the corresponding process.

To find the evolution of the strong coupling with the momentum scale, we start from Eq. (27) and introduce the variable

$$t = \ln(Q^2/\tilde{\mu}^2), \quad (32)$$

where  $Q^2$  is the momentum transferred in a given process. Notice that the reference scale  $\tilde{\mu}$  is usually large enough, so as to make sure that the calculation is well within the perturbative domain, therefore  $Q^2 < \tilde{\mu}^2$ . After this change of variable, the RGE becomes

$$\left( -\frac{\partial}{\partial t} + \alpha_s \beta(\alpha_s) \frac{\partial}{\partial \alpha_s} - \gamma \right) \Pi(q^2; \alpha_s) = 0. \quad (33)$$

Using the method of the characteristics [5], one obtains the relation between the coupling values evaluated at  $Q^2$  and the reference scale  $\mu^2$  as

$$\int_{t(Q^2=\tilde{\mu}^2)}^{t(Q^2)} dt = -\frac{1}{b_1} \int_{\alpha_s(Q^2=\tilde{\mu}^2)}^{\alpha_s(Q^2)} \frac{d\alpha_s}{\alpha_s^2}. \quad (34)$$

Solving for  $\alpha_s(Q^2)$ , we obtain

$$\alpha_s(Q^2) = \frac{\alpha_s(\tilde{\mu}^2)}{1 + b_1 \alpha_s(\tilde{\mu}^2) \ln(Q^2/\tilde{\mu}^2)}, \quad (35)$$

from where it is seen that as  $Q$  increases, the coupling decreases. This behavior is known as *asymptotic freedom* and it is responsible for the fact that strong interaction processes can be computed in perturbation theory when the transferred momentum is large. Conversely, when this momentum is small, the coupling is so large that perturbative calculations become meaningless. This is the so called *non-perturbative*

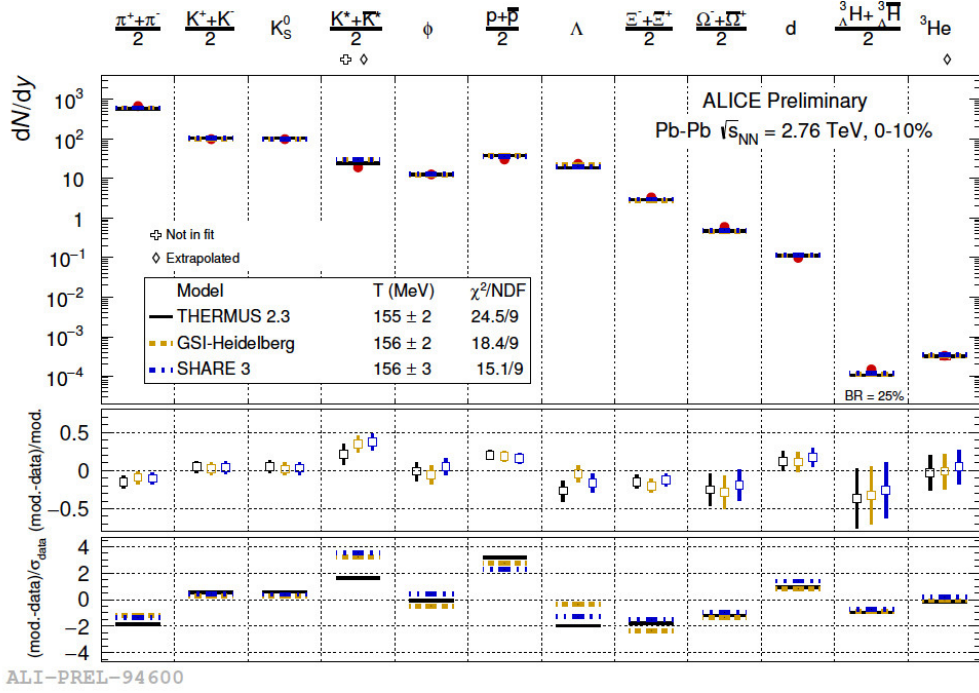


**Figure 5:** Particle ratios obtained in the statistical model compared to experimentally measured ratios in central Pb + Pb collisions at  $\sqrt{s_{NN}} = 2.76$  TeV, obtained by the ALICE Collaboration.

*regime*. Processes where perturbation theory can be applied are usually those where the transferred momentum satisfies  $Q^2 \gtrsim 1 \text{ GeV}^2$ . To quantify this statement, notice that from Eq. (35) we can define a transferred momentum value  $\Lambda_{QCD}$  small enough such that the denominator vanishes and thus the coupling blows up, namely

$$1 + b_1 \alpha_s(\mu^2) \ln(\Lambda_{QCD}^2/\tilde{\mu}^2) = 0, \quad \Lambda_{QCD}^2 = \tilde{\mu}^2 e^{-\frac{1}{b_1 \alpha_s(\tilde{\mu})}} \quad (36)$$

$\Lambda_{QCD}$  is a renormalization scheme dependent quantity. It also depends on the number of active flavors. For instance, in the  $\overline{\text{MS}}$  scheme and for three active flavors, its value is of order  $\Lambda_{QCD} \sim 300 \text{ MeV}$ . All dimensionful QCD results where the transferred momentum is small, scale with  $\Lambda_{QCD}$ . The existence of this scale is the reason for the existence of the mass of baryons and thus of the mass of the visible universe.

The question we now set up to address concerns whether and how heavy-ion reactions allow us to explore the situation where the two above discussed properties of QCD, namely, the breaking of chiral symmetry by the effective quark mass and confinement, can be overcome.

#### 4 Chiral symmetry/deconfinement transitions at high temperature and baryon density

When nuclear matter is subject to extreme conditions, interesting phenomena take place. There are two important parameters when this matter can be described as being in equilibrium: The temperature  $T$  and the baryon number density  $n_B$  (or equivalently its conjugate variable  $\mu_B = 3\mu$ ). Since the intrinsic QCD scale is of order  $\Lambda_{QCD} \sim 200 - 300 \text{ MeV}$ , one expects a transition around  $T \sim \Lambda_{QCD}$  and/or  $n_B \sim \Lambda_{QCD}^3 \sim 1 \text{ fm}^{-3}$ . The temperature and baryon density in a heavy-ion reaction are functions of the center-of-mass energy in the collision.

To estimate the possible values that these quantities achieve, one usually resorts to the *statistical model*. This model assumes that hadron matter is in thermal equilibrium during chemical freeze-out,

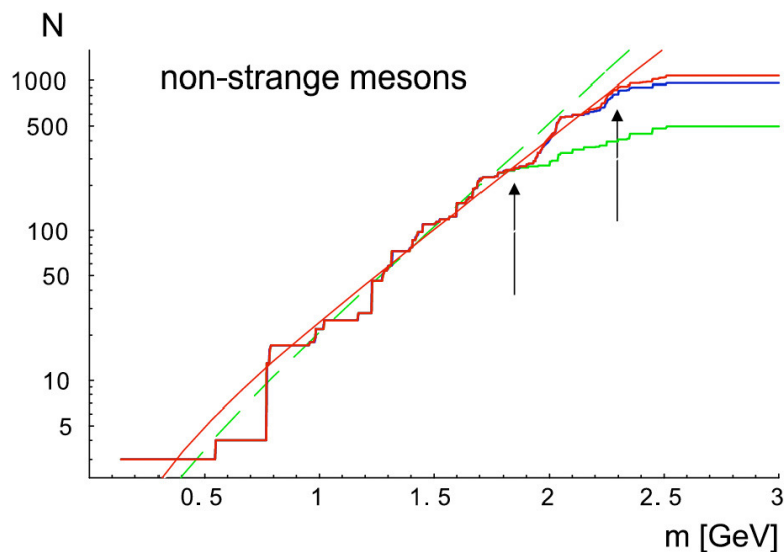


**Figure 6:** Schematic representation of the meson density of states as a function of their mass. Notice that the density of states increases exponentially. Figure taken from Ref. [8].

that is to say, when hadron abundances are established during the reaction. In this manner, it is possible to extract the values for the temperature and baryon chemical potential from fits to particle abundances, given in the model by

$$n_j = \frac{g_j}{2\pi^2} \int_0^\infty p^2 dp \left[ \exp \left\{ \sqrt{p^2 + M_j^2} / T_{ch} - \mu_{ch} \right\} \pm 1 \right]^{-1}, \quad (37)$$

where  $\pm$  refer to fermions and bosons, respectively. Figure 5 illustrates a comparison between the statistical model calculations and experimentally measured particle ratios. The main claim of the model is that since multi-particle scattering rates fall-off rapidly, the experimentally determined chemical freeze-out temperature  $T_{ch}$  and chemical potential  $\mu_{ch}$  are good measures of the phase transition temperature and baryon chemical potential [6].

Using this model, it is found that for central collisions, the baryon chemical potential decreases roughly as the inverse of the center-of-mass energy per nucleon pair in the collision [7]. Therefore, for current collider based experiments where the highest energies are reached, such as the LHC and RHIC, the baryon chemical potential associated to the reaction is the smallest. This can be understood in terms of an increase of the degree of transparency of colliding nuclear matter with collision energy, whereby in the interaction zone, the energy deposited produces roughly an equal number of particles and antiparticles. On the contrary, when the collision energy decreases, the transparency decreases and the reaction zone becomes baryon richer.

A systematic exploration over a wider range of  $n_B$  values, up to several times the normal nuclear matter density  $n_0 \sim 0.16 \text{ fm}^{-3}$ , can be carried out currently by the BES-RHIC and in the future by other facilities such as FAIR, NICA, J-PARC and KEK. In Nature, the interior of compact stellar objects is the relevant system where dense and low temperature QCD matter is realized.

#### 4.1 Phase transitions

A phase transition is a transformation of a given substance from one state of matter to another. During the phase transition some quantities change, often in a discontinuous manner. Changes result from variations of external conditions such as pressure, temperature, etc. In technical terms, a phase transition occurs when the free energy is non-analytic (one of its derivatives diverges) for some values of the thermodynamical variables. Phase transitions result from the interaction of a large number of particles and in general do not occur when the system is very small or has a small number of particles. On the phase transition lines the free energies in both phases coincide. Sometimes it is possible to change the state of a substance without crossing a phase transition line. Under these conditions one talks about a crossover transition.

Phase transitions are classified according to behavior of the free energy as a function of a given thermodynamical variable (Ehrenfest). They are named according to the derivative of lowest order that becomes discontinuous during the transition: First order; the first derivative of free energy is discontinuous. A prototypical example is boiling water. During this process there appears a discontinuity in the density, *i.e.* the derivative of free energy with respect to chemical potential. Second order; the first derivative is continuous but the second derivative is discontinuous. A prototypical example is ferromagnetism. The magnetization, *i.e.* the derivative of the free energy with respect to the external field is continuous. The susceptibility, *i.e.* the derivative of the magnetization with respect to the external field, is discontinuous.

In a modern classification, a first order phase transition involves latent heat. The system absorbs or releases heat at a constant temperature. Phases coexist, although some parts have completed the transition whereas some others have not. A second order phase transition is a continuous transitions. Susceptibilities diverge, correlation lengths become large.

#### 4.2 Deconfinement transition form hadron thermodynamics

Consider an ideal gas of identical neutral scalar particles of mass  $m_0$  contained in a box volume  $V$ . Assume Boltzmann statistics. The partition function and related thermodynamical quantities are given by

$$\begin{aligned}
 \mathcal{Z}(T, V) &= \sum_N \frac{1}{N!} \left[ \frac{V}{(2\pi)^3} \int d^3 p \exp \left\{ -\frac{\sqrt{p^2 + m^2}}{T} \right\} \right]^N \\
 \ln \mathcal{Z}(T, V) &= \frac{VTm_0^2}{2\pi^2} K_2(m_0/T) \\
 \varepsilon(T) &= -\frac{1}{V} \frac{\partial \ln \mathcal{Z}(T, V)}{\partial (1/T)} \xrightarrow{T \gg m_0} \frac{3}{\pi^2} T^4 \quad \text{energy density} \\
 n(T) &= -\frac{1}{V} \frac{\partial \ln \mathcal{Z}(T, V)}{\partial (V)} \xrightarrow{T \gg m_0} \frac{1}{\pi^2} T^3 \quad \text{particle density} \\
 \omega(T) &= \varepsilon(T)/n(T) \simeq 3T \quad \text{average energy per particle}
 \end{aligned} \tag{38}$$

Notice that the above relations imply that an increase of system's energy has three consequences: A higher temperature, more constituents, more energetic constituents.

Let us now include in the analysis hadron resonances whose mass is  $m_i$ . It is easy to show that the partition function is given by

$$\ln \mathcal{Z}(T, V) = \sum_i \frac{VTm_i^2}{2\pi^2} \rho(m_i) K_2(m_i/T), \tag{39}$$

where  $i$  starts with the ground state ( $m_0$ ) and then includes the possible resonances with masses  $m_i$  and  $\rho(m_i)$  is the weight (density of states) corresponding to the state  $m_i$ . It is thus crucial to determine  $\rho(m_i)$ , *i.e.*, how many states there are having mass  $m_i$ .

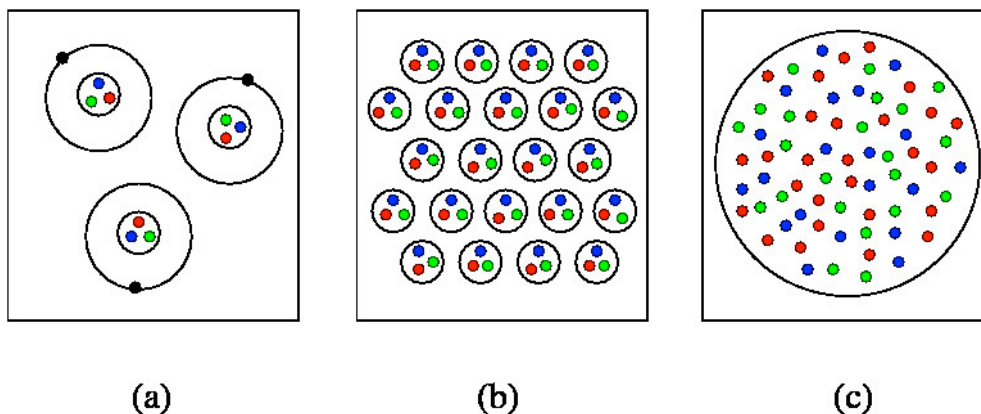


**Figure 7:** Schematic representation of the change of effective degrees of freedom for the description of a set of hadrons when the density and/or temperature increases, as a consequence of a heavy-ion reaction. At low temperatures/densities, the description is given in terms of a collection of hadron resonances. As the temperature/density increases, limiting values of the baryon density and/or temperature are reached above which the descriptions is made in terms of the fundamental QCD degrees of freedom. This signals the onset of a phase transition.

Figure 4 shows a schematic representation of the density of states, albeit for non-strange mesons. In any case, it serves to illustrate that the density of states grows exponentially with the mass of the species,  $\rho(m) \propto \exp\{m/T^H\}$ , where  $T^H \simeq 0.19$  GeV. This exponential growth should be balanced by the Boltzmann factor

$$\exp\left\{\frac{m}{T^H} - \frac{m}{T}\right\}, \quad (40)$$

such that when  $T > T^H$ , the integration over  $m$  becomes singular.  $T^H$  plays the role of a limiting temperature known as the *Hagedorn* temperature above which the hadronic description breaks down.

Applying a similar argument, we can also estimate the critical line at finite  $\mu_B$ . The density of baryon states  $\rho(m_B) \propto \exp\{m_B/T^H\}$ , where  $m_B$  is the typical baryon mass (of order 1 GeV) is balanced by the Boltzmann factor  $\exp\{-(m_B - \mu_B)/T\}$ . The limiting temperature becomes

$$T = \left(1 - \frac{\mu_B}{m_B}\right) T^H. \quad (41)$$

Notice that the treatment of the system as a gas made out of resonances leads to three consequences: More and more species of ever heavier particles appear; a fixed temperature limit  $T \rightarrow T^H$  above which the resonance picture does not hold; the momentum of the constituents do not continue to increase. All in all, these observations imply that above and to the right of the limiting curve, Eq. (41), a different description of hadron matter, in terms of degrees of freedom other than hadron resonances, is called for. The situation is illustrated in Fig. 6. As the system becomes hotter/denser, the boundaries between individual hadrons disappear and the description should be made instead in terms of the fundamental QCD degrees of freedom. A deconfinement phase transition takes place.

### 4.3 Chiral symmetry transition

The QCD vacuum within hadrons should be regarded as a medium responsible for the non-perturbative quark mass. In hot and/or dense matter, quarks turn bare due to asymptotic freedom. We expect a phase transition from a state with heavy constituent quarks to another with light current quarks. This transition is called *chiral phase transition*.

At finite  $T$  and  $\mu$  the QCD phase diagram can also be studied from the point of view of chiral symmetry restoration. In the chiral limit ( $m = 0$ ), a true order parameter for the transition is the *quark-antiquark condensate*  $\langle \bar{\psi}\psi \rangle$ , since it is finite in the chirally broken (Nambu-Goldstone) phase and vanishes in the chirally symmetric (Wigner-Weyl) phase. In this limit the (true) critical temperature can be obtained from the *chiral susceptibility*

$$\chi_m = \frac{\partial}{\partial m} \langle \bar{\psi}\psi \rangle. \quad (42)$$

In vacuum  $\langle \bar{\psi}\psi \rangle_0 = -(0.24 \text{ GeV})^3$ . This value sets the scale for the critical temperature of chiral restoration.

From  $\chi$ PT at low  $T$  and low  $n_B$  one knows that

$$\begin{aligned} \langle \bar{\psi}\psi \rangle_T / \langle \bar{\psi}\psi \rangle_0 &= 1 - T^2 / (8f_\pi^2) - T^4 / (384f_\pi^4) \\ \langle \bar{\psi}\psi \rangle_{n_B} / \langle \bar{\psi}\psi \rangle_0 &= 1 - \sigma_{\pi N} n_B / (f_\pi^2 m_\pi^2) - \dots \end{aligned} \quad (43)$$

where  $f_\pi \simeq 93 \text{ MeV}$ , is the pion decay constant and  $\sigma_{\pi N} = 40 \text{ MeV}$ , is the  $\pi - N$  sigma term. Equations (43) indicate that the quark-antiquark condensate melts at finite  $T$  and  $n_B$ .

For physical quark masses neither  $\langle \bar{\psi}\psi \rangle$  vanishes nor  $\chi_m$  diverges at the pseudocritical temperature. Nevertheless these quantities retain a behavior reminiscent of the corresponding one in the chiral limit. In particular  $\chi_m$  has a peaked structure as a function of  $T$ . It is customary to define  $T_c$  as the temperature for which  $\chi_m$  reaches its peak. Other susceptibilities, such as  $\chi_T = \frac{\partial}{\partial T} \langle \bar{\psi}\psi \rangle$ , can also be used to define  $T_c$ . It has been shown [9] that the critical temperatures thus obtained coincide within a narrow band and therefore using any of these susceptibilities gives basically the same  $T_c$ .

Lattice calculations have provided values for  $T_c$  extracted from the peak of  $\chi_m$  for 2+1 flavors using different types of improved staggered fermions [10]. These values show some discrepancies. The MILC collaboration [11] obtained  $T_c = 169(12)(4) \text{ MeV}$ . The BNL-RBC-Bielefeld collaboration [12] reported  $T_c = 193(7)(4) \text{ MeV}$ . The Wuppertal-Budapest collaboration [13] has consistently obtained smaller values, the latest being  $T_c = 147(2)(3) \text{ MeV}$ . The HotQCD collaboration [14] has reported  $T_c = 154(9) \text{ MeV}$ . The differences could perhaps be attributed to different lattice spacings.

The unambiguous picture presented by lattice QCD for  $T \geq 0$ ,  $\mu = 0$  cannot be easily extended to the case  $\mu \neq 0$ , given that standard Monte Carlo simulations can only be applied to the case where  $\mu$  is either 0 or purely imaginary. Simulations with  $\mu \neq 0$  are hindered by the *sign problem* [15]. Recall that in the computation of the QCD partition function with finite  $\mu$ , integration over each fermion field produces a *fermion determinant*, i.e. a factor  $\text{Det}M \equiv \text{Det}(\not{D} + m + \mu\gamma_0)$ , where  $M$  is the fermion matrix. Let us consider in general a complex  $\mu$ . Taking the determinant on both sides of the identity

$$\gamma_5(\not{D} + m + \mu\gamma_0)\gamma_5 = (\not{D} + m - \mu^*\gamma_0)^\dagger, \quad (44)$$

we get

$$\text{Det}(\not{D} + m + \mu\gamma_0) = [\text{Det}(\not{D} + m - \mu^*\gamma_0)]^*, \quad (45)$$

which shows that the fermion determinant is not real unless  $\mu = 0$  or purely imaginary. For real  $\mu$  the direct sampling of a finite density ensemble by Monte Carlo methods is not possible, since the sampling requires a real non-negative measure. This problem is referred to as the sign problem, although a more appropriate name would seem to be the *phase problem*.

That the integrand of the partition function becomes complex would seem to be only a minor inconvenience. A naive approach to deal with the sign problem would be to write [16]

$$\text{Det}M = |\text{Det}M| e^{i\theta}. \quad (46)$$

## Chiral transition, hadronization and freeze-out

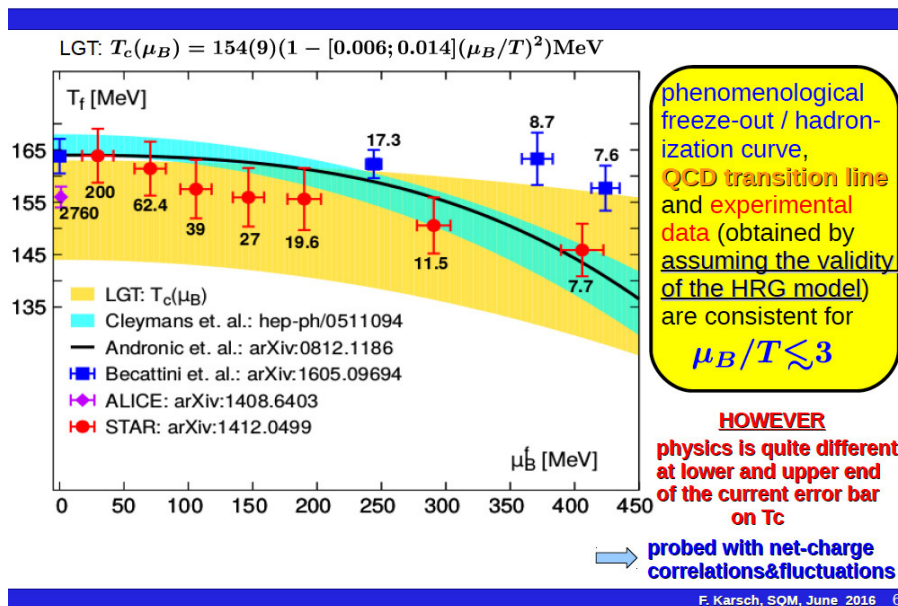


**Figure 8:** Comparison between phenomenological freeze-out curves with the experimentally measured values for the temperature and baryon chemical potential obtained from particle abundances using the statistical model. Shown is also the analytical expression for the chiral phase transition curve obtained by means of LQCD techniques.

To compute the thermal average of an observable  $O$  in QCD one writes

$$\langle O \rangle = \frac{\int DU e^{S_{YM}} \text{Det}M O}{\int DU e^{S_{YM}} \text{Det}M} = \frac{\int DU e^{S_{YM}} |\text{Det}M| e^{i\theta} O}{\int DU e^{S_{YM}} |\text{Det}M| e^{i\theta}}, \quad (47)$$

where  $S_{YM}$  is the Yang-Mills action. Notice that written in this manner, the simulations could be implemented in terms of the phase-quenched (pq) theory where the measure involves  $|\text{Det}M|$  and the thermal average could be written as

$$\langle O \rangle = \frac{\langle O e^{i\theta} \rangle_{\text{pq}}}{\langle e^{i\theta} \rangle_{\text{pq}}}. \quad (48)$$

The average phase factor (also referred to as the average sign) in the phase-quenched theory can be written as

$$\langle e^{i\theta} \rangle_{\text{pq}} = e^{-V(f-f_{\text{pq}})/T}, \quad (49)$$

where  $f$  and  $f_{\text{pq}}$  are the free-energy densities in the full and phase-quenched theories, respectively and  $V$  is the three-dimensional volume. If  $f - f_{\text{pq}} \neq 0$ , the average phase factor decreases exponentially when  $V$  goes to infinity (the thermodynamic limit) and/or  $T$  goes to zero. Under these circumstances the signal to noise ratio worsens. This is referred to as the *severe sign problem*.

To circumvent the sign problem, a possibility is to determine the first Taylor coefficients in the expansion of a given observable in powers of  $\mu_B/T$ . The coefficients of the expansion can be expressed as expectation values of traces of matrix polynomials taken in the  $\mu_B = 0$  ensemble. Although care has to be taken regarding the growth of the statistical errors with the order of the expansion, this strategy has

provided a very important result: the curvature of the transition line at  $\mu_B = 0$ . The curvature  $\kappa$  is defined as the dimensionless coefficient of the quadratic term in the Taylor expansion of the pseudocritical line

$$T_c(\mu_B) = T_c \left( 1 - \kappa \frac{\mu_B^2}{T_c^2} \right), \quad \kappa \equiv - \left( T_c \frac{dT_c(\mu_B)}{d\mu_B^2} \right) \Big|_{\mu_B=0}. \quad (50)$$

Values for  $\kappa$  between 0.006 – 0.02 have been reported [17]. It should be noted that since the phases are separated by a crossover, the curvature should depend in principle on the observable considered. Nevertheless, these curvatures give considerable smaller values than that of the chemical freeze-out curve obtained from statistical models [18]. This observation could be of potential importance for if the pseudo critical line is flatter than the chemical freeze-out line, the distance between the possible QCD critical end point (CEP) and the freeze-out curve increases. If this happens then possible experimental evidences for criticality may be washed out by the moment when particle abundances are established after a heavy-ion collision.

Figure 8 shows a comparison between phenomenological freeze-out curves with the experimentally measured values for the temperature and baryon chemical potential obtained from particle abundances using the statistical model. Shown is also the analytical expression for the chiral phase transition curve obtained by means of LQCD techniques. Although the physics portrayed in the statistical model is quite different from the physics of chiral symmetry restoration, the agreement of the descriptions is remarkable, a similarity that is worth exploring and understanding.

#### 4.4 The critical end point

In the study of the QCD phase diagram, the location of a possible Critical End Point (CEP) is of particular relevance. This point marks the end of a first order phase transition line. There are strong arguments based on effective models suggesting that close to the  $\mu_B$ -axis, the transition is first order [19]. Since, on the other hand, close to the  $T$ -axis, the transition is a smooth crossover, a CEP should be located somewhere in the middle of the phase diagram. To locate its position, the STAR BES-I program has recently analyzed collisions of heavy-nuclei in the energy range  $200 \text{ GeV} > \sqrt{s_{NN}} > 7.7 \text{ GeV}$  [20]. Future experiments [21–23] will keep on conducting an exploration to locate the CEP changing the collision energy down to about  $\sqrt{s_{NN}} \simeq 5 \text{ GeV}$  and the system size in heavy-ion reactions.

From the theoretical side, efforts to locate the CEP make use of a variety of techniques. These involve Schwinger-Dyson equations, finite energy sum rules, functional renormalization methods, holography, and effective models [24–32, 36–38]. These studies have produced a wealth of results for the CEP location that range from low to large values  $\mu_B$  and  $T$ . Recent LQCD analyses [39] have resorted to the imaginary baryon chemical potential technique, extrapolating afterwards to real values, to study the chiral transition near the  $T$ -axis. The method has still large uncertainties, however this technique has shown that the transition keeps being a smooth crossover [40]. The Taylor expansion LQCD technique has also been employed to restrict the CEP's location to values  $\mu_B/T > 2$  for the temperature range  $135 \text{ MeV} < T < 155 \text{ MeV}$ . Its location for temperatures larger than  $0.9 T^c(\mu_B = 0)$  seems to also be highly disfavored [41] (see also [42]).

Table I summarizes the CEP location found in some recent works.

A powerful tool to experimentally locate the CEP is the study of event-by-event fluctuations in relativistic heavy-ion collisions [44]. These are sensitive to the early thermal properties of the created medium. In particular, the possibility to detect non Gaussian fluctuations in conserved charges is one of the central topics in this field.

Let  $n(x)$  be the density of a given charge  $Q$  in the phase space described by the set of variables  $x$ . These quantities are related by

$$Q = \int_V dx n(x), \quad (51)$$

Reference	$T_{CEP}$	$\mu_{CEP}$
C. Shi, <i>et al.</i> [29]	$0.85 T_c$	$1.11 T_c$
G. A. Contrera, <i>et al.</i> [30]	69.9 MeV	319.1 MeV
T. Yokota, <i>et al.</i> [33]	5.1 MeV	286.7 MeV
S. Sharma [34]	145-155 MeV	$> 2 T_{CEP}$
J. Knaute, <i>et al.</i> [36]	112 MeV	204 MeV
N. G. Antoniou, <i>et al.</i> [37]	119-162 MeV	84-86 MeV
Z. F. Cui, <i>et al.</i> [31]	38 MeV	245 MeV
P. Kovács and G. Wolf [35]		$> 133.3$ MeV
R. Rougemont, <i>et al.</i> [38]	$< 130$ MeV	$> 133.3$ MeV
A. Ayala, <i>et al.</i> [43]	18-45 MeV	315-349 MeV

**Table 1:** Summary of some recent results for the CEP location taken from Ref. [43].

where  $V$  is the total phase space volume available. When the measurement of  $Q$  is performed over the volume  $V$  in a thermal system, we speak of a thermal fluctuation. For instance, the variance of  $Q$  is given by

$$\langle \delta Q^2 \rangle_V = \langle (Q - \langle Q \rangle_V)^2 \rangle_V = \int_V dx_1 dx_2 \langle \delta n(x_1) \delta n(x_2) \rangle \quad (52)$$

The integrand on the right hand side of Eq. (52) is called a *correlation function*, whereas the right hand side is called a (second order) *fluctuation*. With this example, we see that fluctuations are closely related to correlation functions. In relativistic heavy-ion collisions, fluctuations are measured on an event-by-event basis in which the number of some charge or particle species is counted in each event. Although these fluctuations are not necessarily equal to the thermal fluctuations, there are good reasons to expect that, with an appropriate treatment these two can be taken as equivalent.

For a probability distribution function  $\mathcal{P}(x)$  of a stochastic variable  $x$ , the moments are defined as

$$\langle x^n \rangle = \int dx x^n \mathcal{P}(x). \quad (53)$$

We can define the *moment generating function*  $G(\theta)$  as

$$G(\theta) = \int dx e^{x\theta} \mathcal{P}(x), \quad (54)$$

from where

$$\langle x^n \rangle = \left. \frac{d^n}{d\theta^n} G(\theta) \right|_{\theta=0} \quad (55)$$

To define the cumulants, it is convenient to define the *cumulant generating function*

$$K(\theta) = \ln G(\theta). \quad (56)$$

The cumulants of  $\mathcal{P}(x)$  are defined by

$$\langle x^n \rangle_c = \left. \frac{d^n}{d\theta^n} K(\theta) \right|_{\theta=0}. \quad (57)$$

It is then possible to write the cumulants in terms of the moments. For instance

$$\langle x \rangle_c = \langle x \rangle,$$

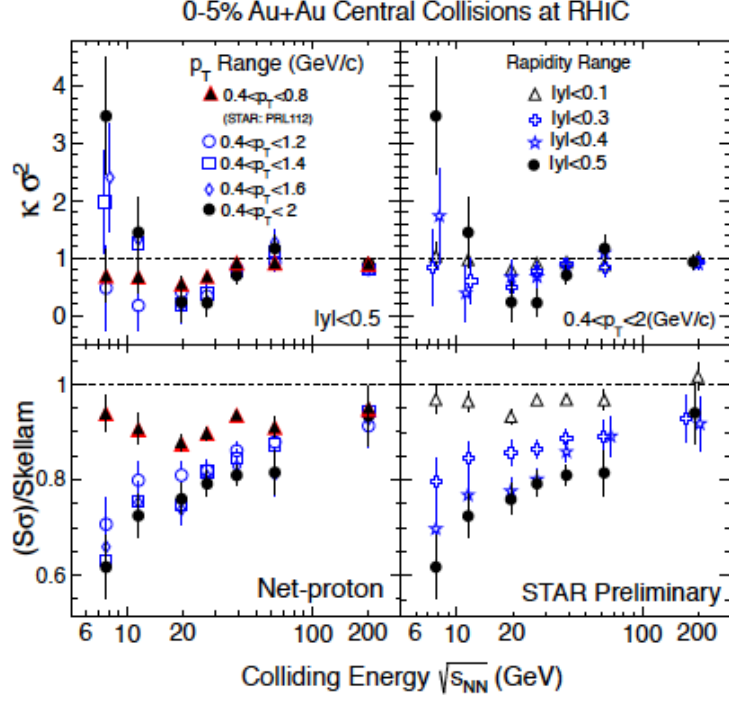


**Figure 9:** Net proton number cumulants measured by STAR. The figure is from Ref. [45].

$$\begin{aligned}
 \langle x^2 \rangle_c &= \langle x^2 \rangle - \langle x \rangle^2 = \langle \delta x^2 \rangle, \\
 \langle x^3 \rangle_c &= \langle \delta x^3 \rangle, \\
 \langle x^4 \rangle_c &= \langle \delta x^4 \rangle - 3 \langle \delta x^2 \rangle^2.
 \end{aligned} \tag{58}$$

The relation with thermodynamics comes through the partition function  $\mathcal{Z}$ , which is the fundamental object. The partition function is also the moment generating function and therefore the cumulant generating function is given by  $\ln \mathcal{Z}$ .

Cumulants are extensive quantities. Consider the number  $N$  of a conserved quantity in a volume  $V$  in a grand canonical ensemble. It can be shown that its cumulant of order  $n$  can be written as

$$\langle N^n \rangle_{c,V} = \chi_n V, \tag{59}$$

where the quantities  $\chi_n$  are called the *generalized susceptibilities*. From the thermodynamical side, the derivatives of  $\ln \mathcal{Z}$  with respect to the chemical potentials give the susceptibilities. For instance

$$\chi_{BQS}^{ijk} = \frac{\partial^{i+k+j}(P/T^4)}{\partial^i(\mu_B/T) \partial^j(\mu_Q/T) \partial^k(\mu_S/T)}; \quad P = \frac{T}{V} \ln \mathcal{Z}. \tag{60}$$

Also, since cumulants higher than second order vanish for a Gaussian probability distribution, non-Gaussian fluctuations are signaled by non-vanishing higher order cumulants.

Two important higher order moments are the *skewness*  $S$  and the *curtosis*  $\kappa$ . The former measures the asymmetry of the distribution function whereas the latter measures its sharpness. When the stochastic

variable  $x$  is normalized to the square root of the variance,  $\sigma$ , such that  $x \rightarrow \tilde{x} = x/\sigma$ , the skewness and the kurtosis are given as the third and fourth-order cumulants, namely

$$S = \langle \tilde{x}^3 \rangle_c, \quad \kappa = \langle \tilde{x}^4 \rangle_c. \quad (61)$$

When fluctuations of conserved charges in relativistic heavy-ion collisions are well described by hadron degrees of freedom in equilibrium, their cumulants should be consistent with models that describe these degrees of freedom, such as the Hadron Resonance Gas (HRG) model. On the other hand, when fluctuations deviate from those in the HRG model, they can be used as experimental signals of non-hadron and/or non-thermal physics. Figure 9 shows that experimental ratios of some cumulants present statistically significant deviations from the HRG model, though within large errors. Near the CEP, higher order cumulants of conserved charges also behave anomalously. In particular, they change sign in the vicinity of the critical point. They are also sensitive to the increase of correlation lengths [46].

## 5 Experimental signatures of deconfinement

The results from relativistic heavy-ion experiments carried out at the largest available energies have produced a picture of the properties of the created matter at high temperatures, though for small baryon chemical potentials. These properties are extracted from observables optimized to probe the evolution of the system during the different stages of the collision. There are many reviews devoted to the detailed description of such observables and their meaning [47]. Here I content myself with a brief review of some of the main characteristics that have been reported and on how these help us providing a coherent picture of the kind of matter produced in these reactions.

During the initial stages of the collision, dense gluon fields create a strongly interacting medium, the initial state is described by the Color Glass Condensate. This Medium rapidly expands and thermalizes; a Quark Gluon Plasma (QGP) is produced which continues to expand and eventually cools down below  $T_c \simeq 155$  MeV where it hadronizes and becomes a hadron-resonance gas. At a very similar temperature (known as chemical freeze-out temperature  $T^{\text{chem}}$ ), the particle composition is fixed. After chemical freeze-out, particles continue to interact. Only their momentum distributions are affected since their energy is below the inelastic reaction threshold. Hadrons then cease to interact at a kinetic freeze out temperature  $T^{\text{kin}} \simeq 95$  MeV, instant when they have developed a radial flow velocity  $\langle \beta_T \rangle \simeq 0.65$ . A summary of the parameters that characterize the produced medium is as follows:

- Temperature: 100 – 500 MeV.
- Volume:  $1 - 5 \times 10^3$  fm<sup>3</sup>.
- Lifetime: 10 – 20 fm/c.
- Pressure: 100 – 300 MeV/fm<sup>3</sup>.
- ensity:  $1 - 10 \rho_0$  ( $\rho_0 = 0.17$  fm<sup>-3</sup> normal nuclear density).

At low  $p_T < 2$  GeV/c, hydrodynamics provides a good description of this bulk properties. Notice that a large fraction of all particles is produced in this  $p_T$  regime. The produced bulk medium behaves like an almost perfect fluid with a value of shear viscosity to entropy ratio  $\eta/s$  close to its lower theoretical value. The medium is opaque to hard probes, quenching their energy. Radial flow tends to deplete the particle spectrum at low values (blue shift), which increases with increasing particle mass and transverse velocity.

In peripheral collisions, an elliptic flow, characterized by the coefficient  $v_2$  of the the azimuthal angle particle distribution's harmonic expansion, develops. The azimuthal distribution can be expressed as

$$\frac{dN}{d(\phi - \Psi_R)} = N_0 [1 + 2v_1(p_T) \cos(\phi - \Psi_R) + 2v_2(p_T) \cos(2(\phi - \Psi_R)) \dots] \quad (62)$$

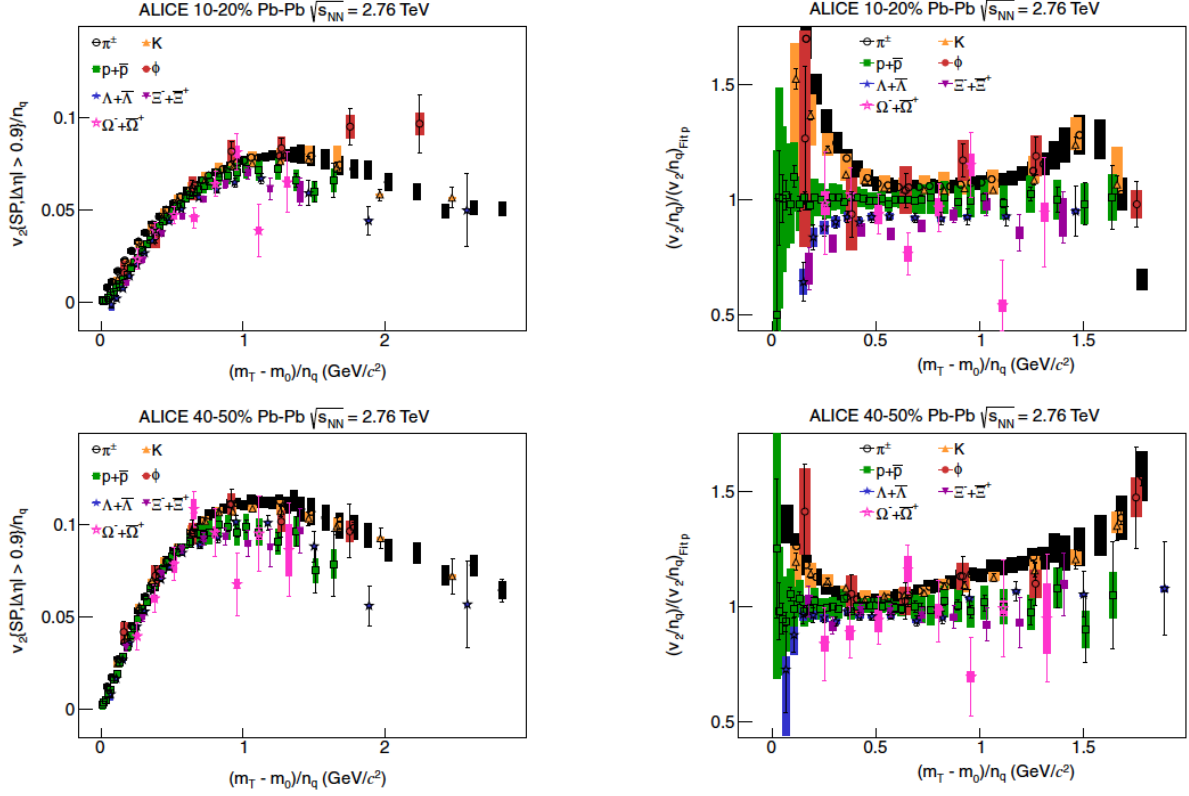


**Figure 10:** Deviations from  $v_2$  scaling with hadron's quark content measured by the ALICE Collaboration. The figure is taken from Ref. [48]

It is believed that  $v_2$  originates from the asymmetric pressure gradients of the initial ellipsoidal overlap region. The strength of this coefficient increases, as expected, with the initial geometric asymmetry from central to peripheral collisions, with maximal value for the centrality range 40–50%. It is interesting to notice that particle depletion becomes larger in-plane than out-of-plane, thereby reducing  $v_2$ . The net result is that at a fixed value of  $p_T$  heavier particles have smaller  $v_2$  than lighter ones.

At RHIC energies, it was reported that at intermediate  $p_T$  if both  $v_2$  and  $p_T$  were scaled by the number of constituent quarks  $n_q$ , the various identified hadrons follow an approximate common behavior. Scaling was interpreted as a signature that quark coalescence was a dominant hadronization mechanism in this momentum domain and also as the onset of the quark degrees of freedom importance during the early stages of heavy-ion collisions, when collective flow develops. However, recent ALICE data shows that scaling, if any, is only approximate, for all centrality intervals. This is illustrated in Fig. 10.

Angular correlations also provide with an important experimental tool to explore collective phenomena. It has been observed that  $\Delta\eta\Delta\phi$  distributions contain two important features: (1) A peak around  $(\Delta\eta, \Delta\phi) = (0, 0)$  (near side peak from jets) and (2) Long-range correlations called ridges (collective phenomena). This is illustrated in Fig. 11. Similar structures are observed in small reference systems. Possible explanations for these observations are either hydrodynamical behavior and/or gluon saturation of the initial state (CGC).

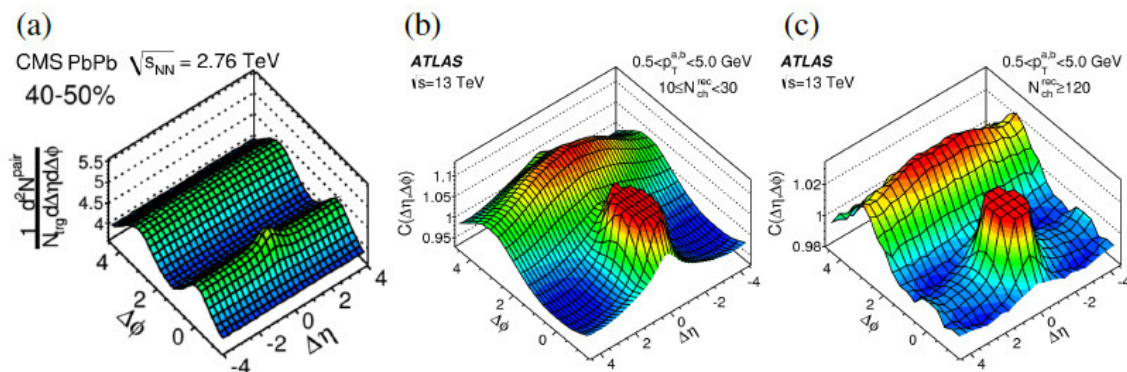


**Figure 11:**  $\Delta\eta\Delta\phi$  distributions in Pb+Pb collisions measured by the CMS and ATLAS Collaboration. The main features of these correlations are visible: A peak around  $(\Delta\eta, \Delta\phi) = (0, 0)$  coming from the near side jet and long-range correlations called ridges, associate to collective phenomena. The figure is from Ref. [49].

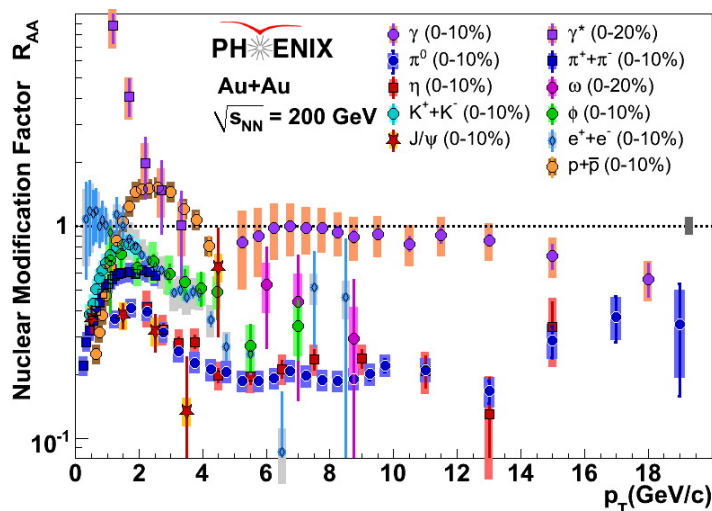


**Figure 12:** Nuclear Modification Factor, for all identified particles measured by PHENIX in central Au+Au collisions at  $\sqrt{s_{NN}}=200$  GeV.

Hard probes such as highly energetic jets of hadrons with heavy flavor content are also a powerful tool to explore the response properties of the medium. An important finding in this context is the observation of the *jet quenching* phenomenon. This is quantified in terms of the *nuclear modification factor*

$$R_{AA}(p_T) = \frac{dN^{AA}(p_T)/dp_T}{\langle N_{col} \rangle dN^{pp}(p_T)/dp_T}. \quad (63)$$

The prototypical behavior of  $R_{AA}$  for several species is illustrated in Fig. 12. Notice that hadrons species show quenching. This quenching is usually attributed to the energy loss suffered by the propagating parton that later on hadronizes. It is important to emphasize that energy loss and elliptic flow are interconnected, that is to say that a clear relationship between jet suppression  $R_{AA}$  and initial nuclear geometry  $v_2$  is observed. This relationship confirms not only the existence of the medium but also the expectation that jet suppression is strongest in the out-of-plane direction where partons traverse the largest amount of hot matter.

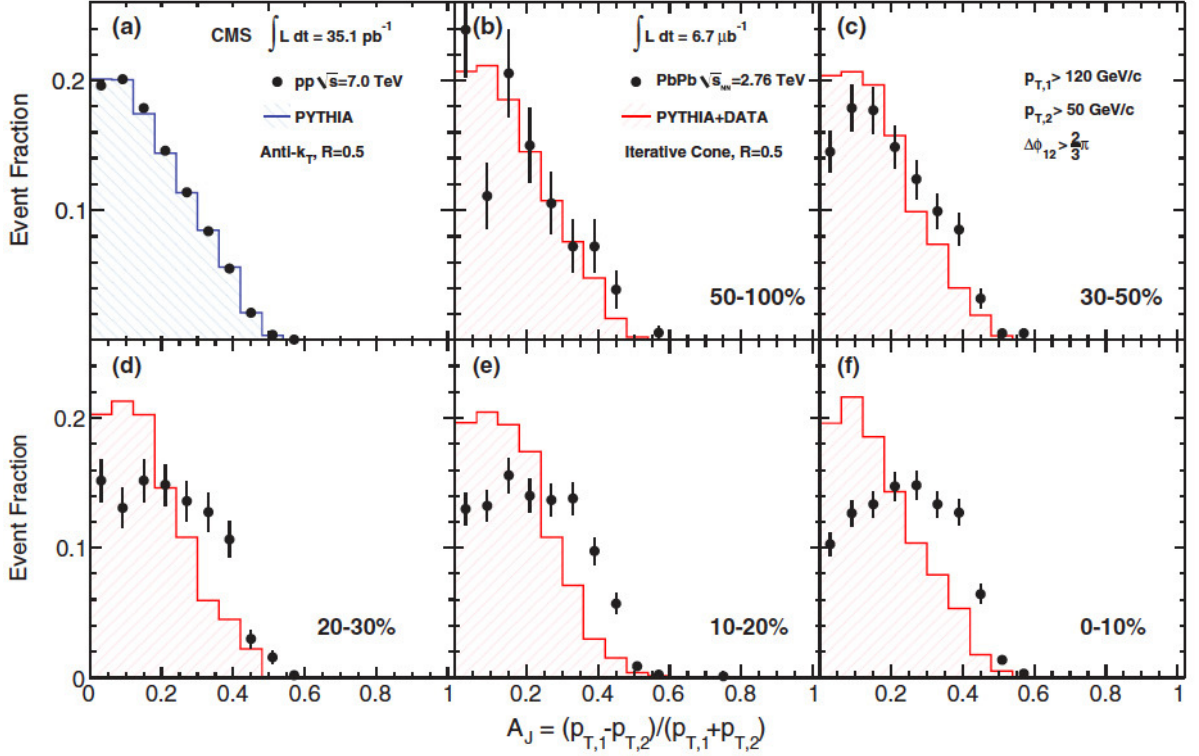


**Figure 13:** Asymmetry distribution as a function of jet asymmetry for p+p and Pb+Pb collisions from CMS data. Notice that for the case of Pb+Pb collisions the peak of the distribution moves to larger jet asymmetries as the centrality of the collision increases. The figure is from Ref. [50].

A pertinent question is, where does the quenched jet energy go? The answer can be quantified in terms of the asymmetry distribution as a function of the jet asymmetry variable

$$A_J = \frac{P_{T,1} - P_{T,2}}{P_{T,1} + P_{T,2}}. \quad (64)$$

When no medium modification is present, near and away-side jets carry similar momentum and the asymmetry distribution peaks for  $A_J \sim 0$ . However, when near and away-side jets carry different amounts of energy, the asymmetry distribution does not peak for  $A_J \sim 0$  anymore. This is illustrated in Fig. 13 where data from CMS on p+p and Pb+Pb data are compared to PYTHIA (no medium present) simulations. The data on Pb+Pb collisions clearly show that the peak of the distribution moves to larger jet asymmetries as the centrality of the collision increases.

To quantify the amount of missing momentum inside away jet, one defines the average missing  $p_T$

$$\langle p_T^{\parallel} \rangle \equiv \frac{1}{N} \sum_{i \in \text{all } N \text{ tracks}} -p_T^i \cos(\phi_i - \phi_L). \quad (65)$$

The momentum in the away-side is obtained for tracks around the sub-leading jet within a cone aperture larger than the jet cone. Data show that the contribution to the momentum around the leading cone comes mostly from tracks with  $p_T > 8$  GeV. This momentum is balanced by the combined contributions from tracks with  $0.5 < p_T < 8$  GeV outside the away-side jet cone with  $\Delta\phi < \pi/6$ . This is shown in Fig. 14

Finally, we mention that another important tool to probe medium properties is the study of heavy flavors. Heavy flavors are produced by initial hard-scattering processes at time scales of order  $\tau \sim 1/2m_H$  (0.07 fm for charm and 0.02 fm for bottom), which are short compared to QGP formation ( $\tau_0 \sim 0.1 - 1$

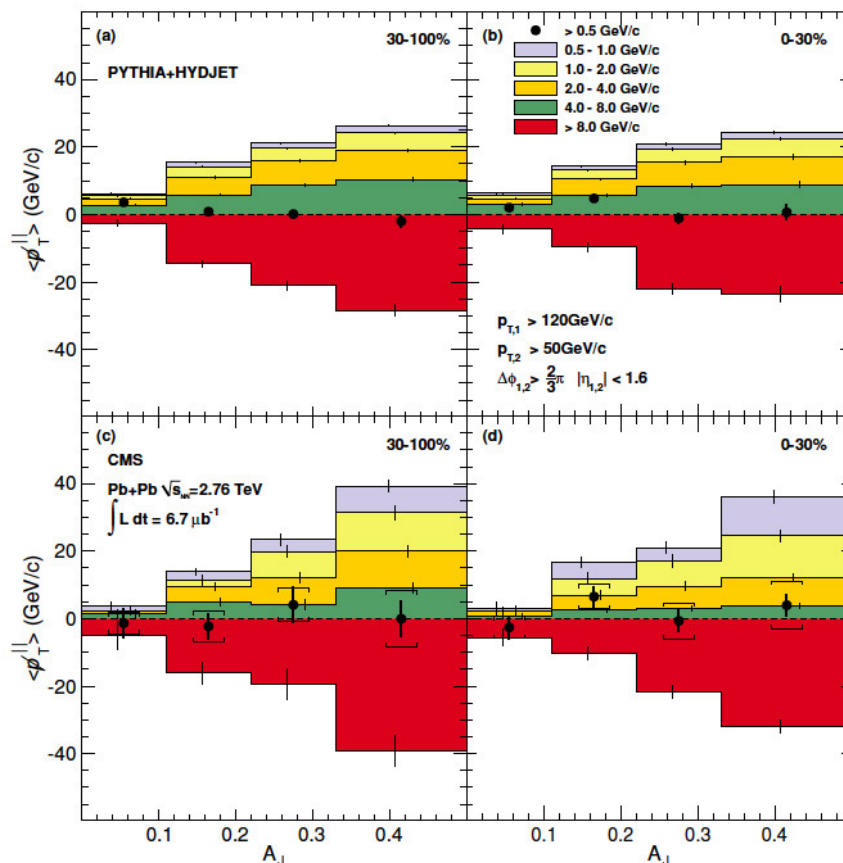
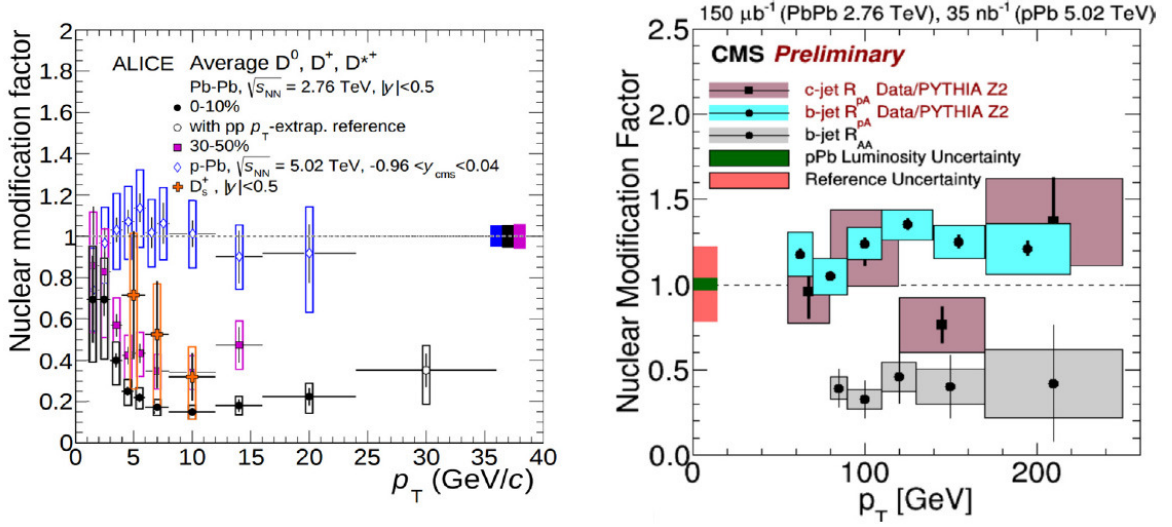


**Figure 14:** Missing  $p_T$ , that is, the sum of the momentum in tracks in the away side with aperture larger than the jet cone. The contribution to the momentum around the leading cone comes mostly from tracks with  $p_T > 8$  GeV and this is balanced by the combined contributions from tracks with  $0.5 < p_T < 8$  GeV outside the away-side jet cone. The figure is from Ref. [50].

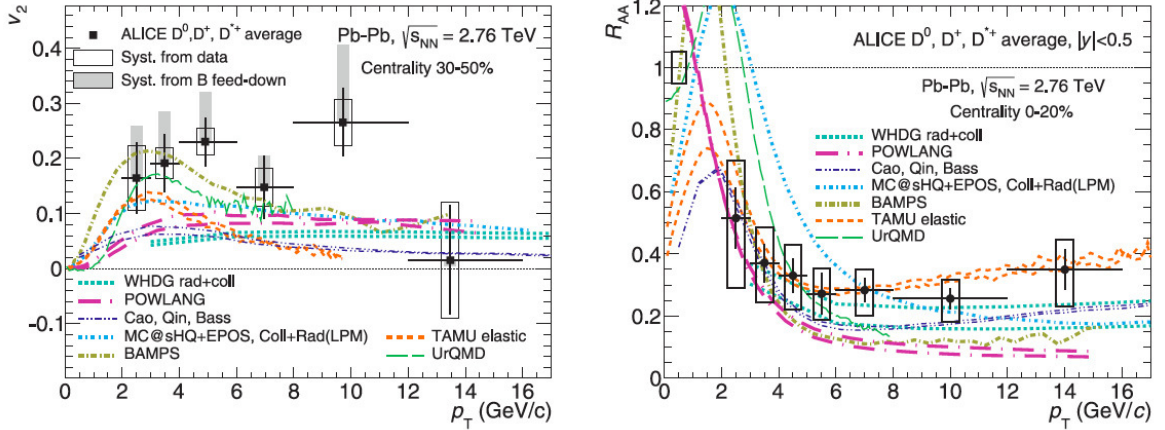
fm). Therefore heavy flavors witness the entire medium evolution. Their annihilation rate in the QGP is small, although interaction with the medium may redistribute their momentum. These characteristics make heavy flavors a good probe for medium properties, that is, for the study of transport coefficients. At the LHC, the production cross section is much larger than at RHIC, thus heavy flavors can be studied more systematically.

Figure 15 shows the quenching pattern for open-flavor heavy-mesons. Notice that in nuclear collisions, the suppression is as strong as for the case of light flavors. This is contrary to the case of p+Pb collisions. A large suppression indicates a strong heavy-flavor coupling with medium. Pure energy loss predicts effects predict a hierarchy in the suppression pattern,  $R_{AA}^{\text{light}} < R_{AA}^D < R_{AA}^B$ . However, one should be cautious since there are a number of effects that may alter such suppression pattern, for instance the differences between primordial spectral shapes of produced partons and their fragmentation functions; the differences between the kinds of processes of flavor production (recall that light flavors are mainly produced by soft processes, whereas heavies are produced by hard processes), etc. The observed agreement  $R_{AA}(D) \simeq R_{AA}(\pi)$  is reproduced by models that include different fragmentation functions and shapes of the primordial  $p_T$  distributions, in addition to the expected energy loss hierarchy. On the other hand, a comparison of  $R_{AA}(D)$  and  $R_{AA}(J/\psi)$  shows the expected suppression pattern.

Heavy-flavor hadrons can share the medium azimuthal anisotropy quantified by  $v_2$ . Data show large  $v_2$  of charm (same magnitude as  $v_2$  of light-hadrons) which implies that charm thermalizes in



**Figure 15:**  $R_{AA}$  for prompt  $D$  mesons as a function of  $p_T$  for Pb+Pb collisions compared to p+p collisions obtained by ALICE (left) and CMS (right) Collaborations. Notice that in nuclear collisions, the heavy-flavor  $R_{AA}$  is comparable to the light flavor one and that in p+Pb collisions it is comparable to 1. The figures are from Refs. [51, 52].



**Figure 16:** Prompt  $D$  mesons  $v_2$  for Pb+Pb collisions at  $\sqrt{s_{NN}} = 2.76$  TeV measured by the ALICE Collaboration. Figures are taken from Ref. [53]

medium. This is illustrated in Fig.16.

As a final remark, we notice that the simultaneous measurements of  $R_{AA}$  and  $v_2$  help to disentangle the interplay of different energy loss scenarios and imposes constraints on theoretical models.

## 6 Conclusions

The heavy-Ion Standard Model is being developed as we speak. For this purpose there is a strong synergy between experiment and theory. Experimental measurements pose many theoretical challenges and rise questions stimulating progress. The field represents a rich and diversity field of approaches. Semi-classical gauge theory for initial conditions, LQCD for static thermodynamic properties, perturbative QCD in vacuum and in-medium, transport theory and particularly viscous hydrodynamics for the evolution of bulk matter and even holographic methods can be employed to describe the dynamics of

thermalization. There is also a large variety of open problems in different fronts: Thermal photon puzzle, extraction of transport coefficients, interplay between hard and soft modes, limit of applicability of hydro approach and inclusion of bulk viscosity in 3D calculations, role of magnetic fields in peripheral collisions, critical point of phase diagram, etc., are only some of the questions that need attention. Overall this is an exciting field with many opportunities to continue exploring the properties of QCD matter under extreme conditions.

## References

### Bibliography

- [1] This section is largely based on H. Sazdjian, Introduction to chiral symmetry in QCD, arXiv:1612.04078.
- [2] M. S. Bhagwat, M. A. Pichowsky, C. D. Roberts, P. C. Tandy, Phys. Rev. C **68**, 015203 (2003).
- [3] P. Pascual and R. Tarrach (1984), QCD: Renormalization for the practitioner. Springer Berlin Heidelberg.
- [4] Michael E. Peskin and Daniel V. Schroeder (1995), An Introduction to Quantum Field Theory, Addison-Wesley Publishing Company, Massachusetts.
- [5] Fritz John (1971). Partial Differential Equations. Springer-Verlag New York.
- [6] See for example: A. Andronic, P. Braun-Munzinger, J. Stachel, Nucl. Phys. A **772**, 167-199 (2006).
- [7] S. K. Tiwari, C. P. Singh, Adv. High Energy Phys. **2013**, 805413 (2013).
- [8] W. Broniowski, W. Florkowski, L. Ya. Glozman, Phys. Rev. D **70**, 117503 (2004).
- [9] X. Shu-Sheng, S. Yuan-Mei, Y. You-Chang, C. Zhu-Fang and Z. Hong-Shi, Chin. Phys. Lett. **32**, 121203 (2015).
- [10] For a review of these results see L. Levkova, PoS Lattice **2011**, 011 (2011).
- [11] C. Bernard *et al.* (MILC Collaboration), Phys. Rev. D **71**, 034504 (2005).
- [12] M. Cheng *et al.*, Phys. Rev. D **74**, 054507 (2006).
- [13] S. Borsányi *et al.*, J. High Energy Phys. 1009.073 (2010); Y. Aoki *et al.*, J. High Energy Phys. 0906.088 (2009); Y. Aoki *et al.*, Phys. Lett. B **643**, 46 (2006).
- [14] A. Bazavov, PoS Lattice **2011**, 182 (2011); A. Bazavov *et al.*, Phys. Rev. D **85**, 054503 (2012).
- [15] For a recent review see P. de Forcrand, PoS Lattice **2009**, 010 (2009).
- [16] G. Aarts, PoS Lattice **2012**, 017 (2012).
- [17] Z. Fodor, C. Guse, S. D. Katz, K. K. Szabo, PoS Lattice **2007**, 189 (2007); O. Kaczmarek, F. Karsch, E. Laermann, C. Miao, S. Mukherjee, P. Petreczky, C. Schmidt, W. Soeldner, W. Unger, Phys. Rev. D **83**, 014504 (2011); G. Endrődi, Z. Fodor, S. D. Katz, K. K. Szabo, J. High Energy Phys. **1104**, 001 (2011); E. Laermann, F. Meyer, M. P. Lombardo, J. Phys. Conf. Ser. **432**, 012016 (2013); P. Cea, L. Cosmai, A. Papa, Phys. Rev. D **89**, 074512 (2014); C. Bonati, M. D’Elia, M. Mariti, M. Mesiti, F. Negro, F. Sanfilippo, Phys. Rev. D **90**, 114025 (2014); C. Bonati, M. D’Elia, M. Mariti, M. Mesiti, F. Negro, F. Sanfilippo, Phys. Rev. D **92**, 054503 (2015); R. Bellwied, S. Borsanyi, Z. Fodor, J. Günther, S. D. Katz, C. Ratti, K. K. Szabo, Phys. Lett. B **751**, 559-564 (2015); P. Cea, L. Cosmai, A. Papa, Phys. Rev. D **93**, 014507 (2016); P. Hegde and H.-T. Ding (for the Bielefeld-BNL-CCNU Collaboration), PoS Lattice **2015**, 141 (2016).
- [18] J. Cleymans, H. Oeschler, R. Redlich, S. Weaton, J. Phys. G **32**, S165 (2006).
- [19] M. Asakawa and K. Yazaki, Nucl. Phys. A **504**, 668 (1989); A. Barducci, R. Casalbuoni, S. De Curtis, R. Gatto and G. Pettini, Phys. Lett. B **231**, 463 (1989); Phys. Rev. D **41**, 1610 (1990); A. Barducci, R. Casalbuoni, G. Pettini and R. Gatto, Phys. Rev. D **49**, 426 (1994); J. Berges and K. Rajagopal, Nucl. Phys. B **538**, 215 (1999); M. A. Halasz, A. D. Jackson, R. E. Shrock, M. A. Stephanov and J. J. M. Verbaarschot, Phys. Rev. D **58**, 096007 (1998); O. Scavenius, A. Mocsy,

- I. N. Mishustin and D. H. Rischke, Phys. Rev. C **64**, 045202 (2001); N. G. Antoniou and A. S. Kapoyannis, Phys. Lett. B **563**, 165 (2003); Y. Hatta and T. Ikeda, Phys. Rev. D **67**, 014028 (2003).
- [20] L. Adamczyk *et al.* [STAR Collaboration], Phys. Rev. Lett. **112**, 032302 (2014); Phys. Rev. Lett. **113**, 092301 (2014).
- [21] C. Yang [for the STAR Collaboration], Nucl. Phys. A **967**, 800-803 (2017).
- [22] P. Senger, J. Phys. Conf. Ser. **798**, 012062 (2017).
- [23] V. Kekelidze, A. Kovalenko, R. Lednicky, V. Matveev, I. Meshkov, A. Sorin, G. Trubnikov, Nucl. Phys. A **967**, 884-887 (2017).
- [24] P. Costa, M. C. Ruivo, and C. A. de Sousa, Phys. Rev. D **77**, 096001 (2008).
- [25] A. Ayala, A. Bashir, C. A. Dominguez, E. Gutierrez, M. Loewe, A. Raya, Phys. Rev. D **84**, 056004Z (2011).
- [26] X.-Y. Xin, S.-X. Qin, Y.-X. Liu, Phys. Rev. D **90**, 076006 (2014)
- [27] C. S. Fischer, J. Luecker and C. A. Welzbacher, Phys. Rev. D **90**, 034022 (2014).
- [28] Y. Lu, Y.-L. Du, Z.-F. Cui, H.-S. Zong, Eur. Phys. J. C **75**, 495 (2015).
- [29] C. Shi, Y.-L. Du, S.-S. Xu, X.-J. Liu, H.-S. Zong, Phys. Rev. D **93**, 036006 (2016).
- [30] G. A. Contrera, A. G. Grunfeld, D. Blaschke, Eur. Phys. J. A **52**, 231 (2016).
- [31] Z.-F. Cui, J.-L. Zhang, H.-S. Zong, Sci. Rep. **7**, 45937 (2017).
- [32] S. Datta, R. V. Gavai, S. Gupta, Phys. Rev. D **95**, 054512 (2017).
- [33] T. Yokota, T. Kunihiro and K. Morita, arXiv:1611.06669 [hep-ph].
- [34] S. Sharma [Bielefeld-BNL-CCNU Collaboration], Nucl. Phys. A **967**, 728 (2017).
- [35] P. Kovács and G. Wolf, Acta Phys. Polon. Supp. **10**, 1107 (2017).
- [36] J. Knaute, R. Yaresko and B. Kämpfer, arXiv:1702.06731 [hep-ph].
- [37] N. G. Antoniou, F. K. Diakonou, X. N. Maintas and C. E. Tsagkarakis, arXiv:1705.09124 [hep-ph].
- [38] R. Rougemont, R. Critelli, J. Noronha-Hostler, J. Noronha and C. Ratti, Phys. Rev. D **96**, no. 1, 014032 (2017).
- [39] P. Cea, L. Cosmai, A. Papa, Phys. Rev. D **93**, 014507 (2016); C. Bonati, M. D'Elia, M. Mariti, M. Mesiti, F. Negro, F. Sanfilippo, Phys. Rev. D **92**, 054503 (2015).
- [40] R. Bellwiede, S. Borsanyi, Z. Fodor, J. GÅijnther, S. D. Katz, C. Ratti, K. K. Szabo, Phys. Lett. B **751**, 559-564 (2015).
- [41] A. Bazavov, *et al.*, Phys. Rev. D **95**, 054504 (2017).
- [42] C. Schmidt and S. Sharma, J. Phys. G **44**, 104002 (2017).
- [43] A. Ayala, L. Hernandez, S. Hernandez-Ortiz, Rev. Mex. Fis. **64**, 302-313 (2018).
- [44] M. Asakawa, M. Kitazawa, Prog. Part. Nucl. Phys. **90**, 299-342 (2016).
- [45] X. Luo [STAR Collaboration], PoS CPOD 2014, 019 (2015).
- [46] M. A. Stephanov, Phys. Rev. Lett. **102**, 032301 (2009).
- [47] P. Foka and M. A. Janik, Rev. Phys. **1**, 154 (2016); *ibid* **1**, 172 (2016).
- [48] F. Noferini (for the ALICE Collaboration), Eur. Phys. Jour. Web of Conf. **90**, 08005 (2015).
- [49] S. Chatrchyan, *et al.*, Eur. Phys. J. C **72** (2012) 2012.
- [50] S. Chatrchyan *et al.* (CMS Collaboration), Phys. Rev. C **84**, 024906 (2011).
- [51] J. Adam, D. Adamová *et al.* (ALICE Collaboration), J. High Energy Phys. **2016**, 81 (2016).
- [52] QM2015, Nucl. Phys. A **956**, 1âĀš974 (2015).
- [53] N. Armesto, E. Scomparin, Eur. Phys. J. Plus **131** (3), 52 (2016).